A theoretical insight into low-temperature atmospheric-pressure He+H_2 plasmas

2013 Plasma Sources Sci. Technol. 22 055016

(http://iopscience.iop.org/0963-0252/22/5/055016)

Plasma Sources Sci. Technol. **22** (2013) 055016 (12pp) doi:10.1088/0963-0252/22/5/055016

A theoretical insight into low-temperature atmospheric-pressure He+H_2 plasmas

Ding-Xin Liu[1], Felipe Iza[2], Xiao-Hua Wang[1], Zhi-Zhen Ma[1], Ming-Zhe Rong[1] and Michael G Kong[1,3]

[1] State Key Laboratory of Electrical Insulation and Power Equipment, Xi'an Jiaotong University, Xi'an 710049, People's Republic of China
[2] School of Electronic, Electrical and Systems Engineering, Loughborough University, LE11 3TU, UK
[3] Frank Reidy Center for Bioelectrics, Department of Electrical & Computer Engineering, Old Dominion University, Norfolk, VA 23508, USA

E-mail: mzrong@mail.xjtu.edu.cn

Received 11 March 2013, in final form 10 July 2013
Published 26 August 2013
Online at stacks.iop.org/PSST/22/055016

Abstract

H_2-containing low-temperature plasmas are used in a wide range of industrial applications. In recent decades, efforts have been made to understand and improve the performance of these plasmas, mainly when operated at low and medium pressures. Studies of hydrogen-containing plasmas at atmospheric pressure, however, are scarce despite the potential advantage of operation in a vacuum-free environment. Here the chemistry of low-temperature atmospheric-pressure He + H_2 plasmas is studied by means of a global model that incorporates 20 species and 168 reactions. It is found that for a fixed average input power the plasma density decreases sharply when the H_2 concentration is higher than ~0.2%, whereas the atomic H density peaks at a H_2 concentration of ~2%. Operation at larger H_2 concentrations leads to lower plasma densities and lower H concentrations because at high H_2 concentrations significant power is dissipated via vibrational excitation of H_2 and there is an increasing presence of negative ions (H^-). Key plasma species and chemical processes are identified and reduced sets of reactions that capture the main physicochemical processes of the discharge are proposed for use in computationally demanding models. The actual waveform of the input power is found to affect the average density of electrons, ions and metastables but it has little influence on the density of species requiring low energy for their formation, such as atomic hydrogen and vibrational states of hydrogen.

(Some figures may appear in colour only in the online journal)

1. Introduction

H_2-containing low-temperature plasmas display strong reducibility, high diffusivity and slight electronegativity, finding use in a wide range of industrial applications, such as cleaning and passivation of oxide layers [1, 2], silicon crystallization [3], polymerization [4, 5], etching [6], plasma addressed liquid crystal displays [7] and growth of nanotubes (mixed with CH_4 or CF_4 as a carbon source) [8, 9]. In recent decades, efforts have been made to understand and improve the performance of these plasmas, mainly when operated at low and medium pressures. Studies of hydrogen-containing plasmas at atmospheric pressure, however, are scarce despite the potential advantage of operation in a vacuum-free environment.

In this paper, low-temperature atmospheric-pressure He + H_2 plasmas are studied by means of a global model. Global models have been widely used to study the chemistry of low-pressure [10–12] and atmospheric-pressure [13–16] plasmas, as they provide a computationally effective way of analysing plasma chemistry and identifying key chemical pathways. Global models of atmospheric-pressure He+O_2, He+H_2O and He+O_2+H_2O plasmas have been reported in recent years and qualitative agreement has been found between computational results and experimental observations made via optical spectroscopy and mass spectrometry [14–17]. The

He+H_2 model used in this study incorporates 20 plasma species and 168 chemical reactions, which have been compiled from an extensive literature review.

Results are presented for a wide range of H_2 concentrations (1 ppm up to 50%) and due to their application relevance, special attention is paid to the density and generation mechanisms of H and H^-. Vibrational excitation of H_2 is also discussed as significant differences are found when comparing atmospheric-pressure He+H_2 discharges with their low-pressure counterparts. In addition, the power modulation effect on the plasma-induced species is discussed for four input power waveforms.

The paper is structured as follows. A description of the global model is given in section 2, and simulation results for a sinusoidal input power are presented in section 3, where density trends, generation/loss mechanisms of selected species and power dissipation are discussed as a function of the H_2 concentration. Key plasma species and chemical pathways are also identified and reduced sets of reactions and plasma species are proposed for computationally intense models. Finally, in section 4, the influence of the time variation of the input power on the density of plasma species is discussed.

2. Computational model

Here we consider a global model of a discharge sustained between two parallel-plate circular electrodes with a radius of 1 cm and a gap of 2 mm between them. The He+H_2 discharge is sustained at atmospheric pressure and is excited by a radio frequency (RF) source (13.56 MHz) that delivers an average power density of 40 W cm^{-3}. The neutral gas temperature is assumed to remain at room temperature (300 K), and the gas flow rate is set to 100 sccm. These conditions are the same as those used in similar computational studies of other atmospheric-pressure discharges and they reflect conditions encountered in actual experiments [14–16]. The H_2 concentration in the feed gas is varied between 1 ppm and 50%, covering a wide range of He/H_2 admixtures relevant for applications.

Global models solve particle and power balance equations and they have been widely used to study the chemistry of low-pressure [12, 18] and atmospheric-pressure [13–16] plasmas. They are zero-dimensional models that neglect spatial variations by describing the plasma in terms of average quantities. As a result, global models are computationally inexpensive and they can easily handle large sets of chemical reactions. Due to these simplifications and the uncertainty in some reaction rates, results of global models typically provide insights into key underlying chemical pathways in a qualitative manner.

The particle balance equation for each plasma species is given by [14]

$$\frac{\mathrm{d}n_k}{\mathrm{d}t} = G_k + \frac{S}{V}\left(\sum_{i=1,i\neq k}^{N} \alpha_{i,k}\Gamma_i - \beta_k\Gamma_k\right) - \frac{F}{V}n_k \qquad (1)$$

where n_k (cm^{-3}) is the number density of species k, G_k (cm^{-3} s^{-1}) is the net generation/loss rate of species k due to reactions in the bulk plasma, N is the total number of species, S (cm^2) is the total area of the electrodes, V(cm^3) is the plasma volume, Γ_k (cm^{-2} s^{-1}) is the flux of species k to the electrodes, $\alpha_{i,k}$ is the probability of producing species k by a reaction on the electrode from species i, β_k is the surface loss probability of species k and F is the gas flow rate (sccm). The first term on the right-hand side represents volume processes, the second term the particle gain/loss due to surface reactions on the electrodes and the third term the loss due to gas flow. Losses of species on the boundaries are dealt with as described in detail in previous works [14]. In brief, the negative ions are assumed to be confined by the ambipolar field, i.e. $\Sigma\Gamma_- = 0$, and the electron loss balances the positive ion flux thereby keeping the plasma quasi-neutral. Although atmospheric-pressure sheath-dominated discharges in which quasi-neutrality does not hold have been reported in the literature, these occur in discharges with a smaller gap than the 2 mm considered in this study [19, 20]. Diffusion in the radial direction is neglected here since the mean distance travelled by particles during their lifetime is much shorter than the radius of the electrodes [14, 21]: for a typical lifetime (τ) of 1 ms and a diffusion constant (D) of 1 cm^2 s^{-1}, the distance travelled is $\sqrt{D\tau} < 3 \times 10^{-2}$ cm, which is much smaller than the electrode radius (1 cm).

Reaction rates needed to determine the generation/loss of species in the discharge (G_k) depend on the mean electron energy. This is determined by solving the power equation [11, 14]. Typically, it is assumed that the power delivered to the plasma is mainly coupled to electrons although various schemes have been proposed to account also for power dissipation in the sheaths [10–14]. Here we follow the approach used in [14]. In addition, it is noted that a significant amount of power can be coupled to ions in the bulk plasma of an atmospheric-pressure discharge. The ratio of power coupled to ions in the bulk to the total (electrons + ions) power coupled to the bulk plasma is given by [21]

$$r = \frac{\sum_k \mu_\mathrm{i}^k n_\mathrm{i}^k}{\mu_\mathrm{e} n_\mathrm{e} + \sum_k \mu_\mathrm{i}^k n_\mathrm{i}^k} \qquad (2)$$

where μ_e (cm^2 V^{-1} s^{-1}) is the electron mobility, n_e (cm^{-3}) is the electron density, μ_i^k(cm^2 V^{-1} s^{-1}) is the mobility of ionic species k and n_i^k (cm^{-3}) is the density of ionic species k. In electropositive discharges, the electron density is comparable to the ion density and due to its larger mobility most of the current in the bulk is carried by electrons and hence most of the power is coupled to the electrons. However, if the discharge becomes electronegative, the electron density will be smaller than the ion density and the ion current in the bulk may not be negligible when compared with the electron current. For a He+H_2 plasma, we can take H_3^+ as a representative ion. Its mobility is 40 cm^2 V^{-1} s^{-1} and that of the electrons is 1056 cm^2 V^{-1} s^{-1} [22, 23]. Therefore, according to equation (2) even when the densities of electrons and ions are equal, ~4% of the power dissipated in the bulk is coupled to the ions. Taking into consideration the energy coupled to ions in the bulk plasma, the electron power balance

equation can be written as

$$\frac{\mathrm{d}}{\mathrm{d}t}\left(\frac{3}{2}n_{\mathrm{e}}T_{\mathrm{eff}}\right) = \frac{P_{\mathrm{in}}}{eV}(1-r) - \sum_{i=1}^{N_r}\varepsilon_i R_i - \frac{S_1}{V}\left(\varepsilon_{\mathrm{e}}\Gamma_{\mathrm{e}} + \sum_{j=1}^{N_{\mathrm{p}}}\varepsilon_{\mathrm{p}}\Gamma_{1j}\right) \quad (3)$$

where e is the elementary charge, T_{eff} (eV) is the effective electron temperature, P_{in} (W) is the input power, N_r is the number of electron impact reactions, ε_i (eV) and R_i ($\mathrm{cm^{-3}\,s^{-1}}$) are the electron energy loss due to the ith electron impact reaction (including electron–neutral momentum transfer collision) and the corresponding reaction rate, ε_{e} (eV) and ε_{p} (eV) are the energy lost per electron and ion escaping the plasma across the sheaths. Given the large collisionality of atmospheric-pressure discharges, the electron energy relaxation time is short and the electron temperature is expected to be markedly time-modulated. The actual waveform of the instantaneous power, however, is unknown *a priori* and for a fixed input voltage it will vary depending on the plasma density and discharge geometry [24]. For simplicity, results presented in section 3 assume that the input power varies as $P(t) = \frac{\pi}{2}P_{\mathrm{ave}}|\sin(\omega t)|$, where P_{ave} is the phase-averaged input power. A discussion on other time variations of the input power can be found in section 4.

Equations (1) and (3) are integrated using a self-developed MATLAB code that makes use of the built-in stiff ordinary differential equation solver *ode23s* to solve for the evolution of the electron temperature and species densities [25]. The time resolution is chosen so that the rf modulation is accurately captured and the simulations are run until the relative change in phase-averaged densities between consecutive cycles is less than 10^{-4}. For a further description of the model, the reader is directed to [11, 14]. The model considers 20 species and 168 reactions that have been identified after an extensive literature review. The species incorporated in the model are listed in table 1, and a list of the reactions can be found in table A1 in the appendix. Vibrationally excited states $H_2(v)$ and Rydberg states $H_2(R)$ are taken into account to investigate their effect on H^- formation and power dissipation. H_5^+ and larger cluster ions are not considered in this model due to the lack of reliable data. Reaction rate coefficients are either taken from the literature or calculated from cross-section data using Bolsig+ [26], a Boltzmann solver. In the latter case, look-up tables of the reaction rates as a function of the mean electron energy and gas composition are generated and fed to the global model. In a few instances, where data were not available, educated estimates have been made based on the recommendations given in [27, 28]. Some cross-sections for excited states of H_2 have also been estimated by shifting cross-sections of the ground state by the threshold energy, as suggested in [12].

3. Simulation results and analysis

3.1. Density of plasma species as a function of H_2 concentration

The phase-averaged density of charged species in He+H_2 plasmas as a function of H_2 concentration is shown in figure 1. The densities of He^+ and H_2^+ are very small and they are not shown in the figure. At low H_2 concentrations ($[H_2] < 10$ ppm), the dominant ionic species are He_2^+, HeH^+ and H^+, whereas at higher hydrogen concentrations H_3^+ becomes the dominant ion. This trend is similar to that observed in He+N_2 [29], He+O_2 [14], He+H_2O [15, 30] atmospheric-pressure discharges and it can be concluded that unless very high purity He is used (>99.999%), cluster ions will be the dominant ionic species in He atmospheric-pressure discharges.

The electron density is found to increase initially with the addition of hydrogen into the discharge, reaching a maximum at $[H_2] \sim 20$ ppm. The dependence of electron density on the hydrogen concentration, however, is fairly weak as long as the latter remains less than ~0.2%. At higher hydrogen concentrations, the electron density decreases rapidly (figure 1) due to the increasing energy lost in vibrational excitation (see further discussion in section 3.3). It is noted that in experimental studies, a small fraction of H_2 around 1% is often introduced as a means to measure the electron density by Stark broadening of the H_β line [31–33]. If the electron density of an atmospheric-pressure helium discharge is to be measured, however, introducing less than 0.2% of hydrogen is recommended in order to minimize the change in electron density caused by the presence of hydrogen.

Table 1. The 20 species included in the global model.

Species	Model[a]	Species[b]	Model
He	S	He^*	S
H_2	S	He_2^*	S
E	S	H	S
He^+	S1	$H(n=2)$	
He_2^+	S1	$H(n=3)$	
HeH^+	S1	$H_2(v=1)$	S
H^+	S	$H_2(v=2)$	S
H_2^+	S	$H_2(v=3)$	S
H_3^+	S	$H_2(v'')$	S2
H^-	S2	H_2(R)	

[a] S1: species relevant only in regime 1 ($[H_2] < 0.5\%$); S2: species relevant only in regime 2 ($[H_2] > 0.5\%$); S: main species in both regimes 1 and 2.
[b] $H_2(v'')$ represents vibrational excited states of $H_2(v \geqslant 4)$; H_2(R) represents Rydberg states of H_2.

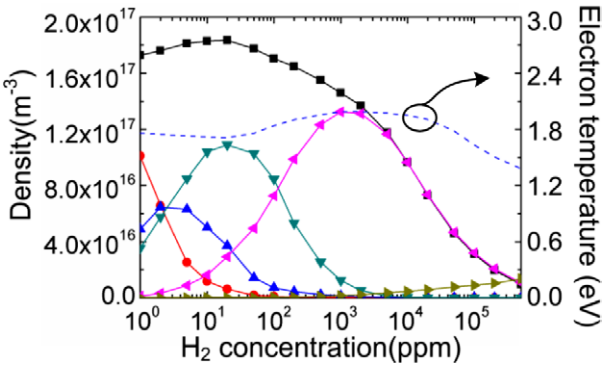

Figure 1. Density of charged species as a function of H_2 concentration; ■: electron; ●: He_2^+; ▲: HeH^+; ▼: H^+; ◀: H_3^+; ▶: 100×H^-; dashed line: electron temperature.

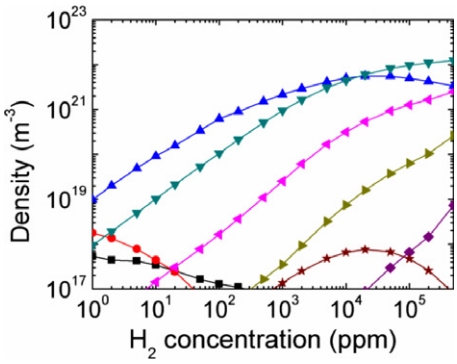

Figure 2. Density of neutral species as a function of H_2 concentration; : He^*; : He_2^*; : H; : $H_2(v = 1)$; : $H_2(v = 2)$; : $H_2(v = 3)$; : $H_2(v'')$; : $10^6 \times H_2(R)$.

As shown in figure 1, the main anion is H^- and its density increases with increasing concentration of H_2 in the discharge. The ratio $[H^-]/[e]$, however, is typically <1 for the conditions considered in this study and therefore the discharge remains electropositive. The phase-averaged electron temperature is also shown in figure 1. The electron temperature remains fairly constant for hydrogen concentrations of up to ~1% and then it decreases due to the lower ionization threshold of H_2 (15.4 eV instead of 24.6 eV required for helium). The variations at a low hydrogen concentration ($[H_2] < 1\%$) are attributed to the varying significance of Penning processes.

Figure 2 shows the phase-averaged density of the most abundant neutral species as a function of H_2 concentration. Species not listed in figure 2 have densities smaller than 10^{17} m^{-3}. The densities of helium (atomic and dimer) metastables decrease sharply with increasing H_2 concentration, whereas the densities of vibrationally excited H_2 increase. At hydrogen concentrations smaller than 1% (10^4 ppm), H atoms are the most abundant neutral species (after the ground state background gases). At higher H_2 concentrations, however, vibrationally excited H_2 becomes more abundant. The density of vibrationally excited states in He+H_2 plasmas is found to be larger than in similar He+O_2 discharges [14] and the implications in terms of plasma chemistry and energy dissipation are discussed in section 3.4. Finally, it is noted that the Rydberg states of H_2 have a similar trend as atomic hydrogen, with a maximum density at $[H_2]$ ~1% but with a density that is ~9 orders of magnitude smaller.

Atomic hydrogen is believed to be critical in many applications of hydrogen-containing plasmas, such as passivation of oxide surface layer [1], silicon crystallization [3], etching [6] and air purification [34]. Therefore, an optimum feed gas composition for atmospheric-pressure He + H_2 plasmas would be He+2%H_2 as this would maximize the density of atomic H. Furthermore, limiting the concentration of H_2 to 2% would mitigate the risk of flame and/or explosion [35].

3.2. Generation and loss mechanisms of electrons, H^- and H

As shown in figure 3(*a*), electron generation is primarily due to Penning processes and the main electron loss mechanism is the loss to the electrodes (figure 3(*b*)). This trend is similar to that observed in other helium-based atmospheric-pressure plasmas [14–16, 29]. The rate of Penning ionization increases with increasing H_2 concentration as more H_2 becomes available for collisions with metastable helium atoms and dimers, reaching a maximum rate at $[H_2]$ ~1000 ppm. At very high H_2 concentration, dissociative attachment (mainly (R50): $e+H_2 \rightarrow H+H^-$) and collisional detachment (mainly (R73): $H^- + H \rightarrow H_2 + e$) become important, resulting in an electron energy loss channel with H^- as an intermediate. At this high H_2 concentration (>5%), electron impact ionization is more effective than Penning processes.

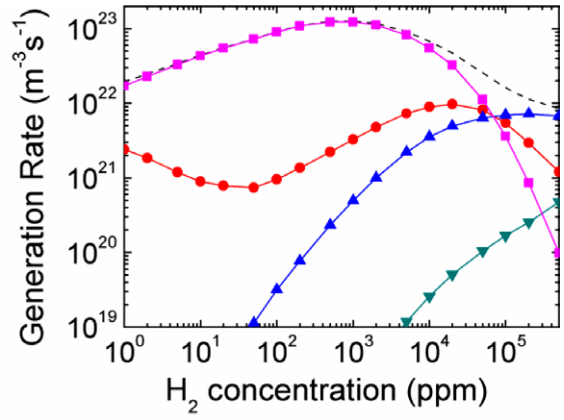

Figure 3. Processes contributing to (*a*) generation and (*b*) loss of electrons; - - - -: total rate; : electron impacted ionization; : $H^- + H \rightarrow H_2 + e$; : collisional detachment by $H_2(v)$; : Penning ionization; : dissociative attachment of H_2; : dissociative attachment of $H_2(v)$; : dissociative attachment of $H_2(R)$; : electron–ion recombination; : electrode loss.

The non-monotonic trend of the electron impact ionization rate shown in figure 3(*a*) reflects the variations in electron temperature shown in figure 1. At $[H_2] < 20$ ppm, Penning processes become more efficient with increasing H_2 concentration, leading to a reduction in the mean electron energy required to sustain the plasma (figure 1) and thereby a decrease in the electron impact ionization rate. The decreasing

trend observed at H_2 concentrations beyond 1% is attributed to the lower electron density present in the discharge at a high H_2 concentration (figure 1).

It is noted that dissociative attachment of vibrationally excited $H_2(v)$ and $H_2(R)$ plays a limited role in the electron density balance (figure 3(*b*)). This is due to the high collisionality of atmospheric plasmas, which results in rapid collisional quenching of energetic states. As a result, dissociative attachment in atmospheric-pressure He+H_2 plasmas plays a much lower role in the electron balance than in low-pressure H_2-containing plasmas [36].

The main production mechanism of H^- in hydrogen-containing plasmas remains unclear [37, 44] and in low-pressure discharges it is normally attributed to the following two processes [36]:

$$e + H_2(v) \rightarrow H + H^- \qquad \text{(R51–54)}$$

$$e + H_2(R) \rightarrow H + H^-. \qquad \text{(R55)}$$

Regarding the dissociative attachment of vibrationally excited $H_2(v)$ (R51)–(R54), it is found that the process is dominated by the dissociative attachment of high-energy states, i.e. $H_2(v'')$. This agrees with the trend observed in medium-pressure hydrogen discharges [7]. The rate coefficients for reactions (R51)–(R55), however, are not well defined and this has contributed to the controversy over the main mechanism leading to H^- production. Here we have assumed that the rate of (R55) is 6×10^{-5} cm^3 s^{-1}, one of the largest values reported in the literature [37], and found that the contribution of Rydberg states is three orders of magnitude lower than that of ground state H_2. The dissociative attachment of $H_2(v'')$ is also small, even smaller than that of low-energy vibrationally excited H_2, i.e. $H_2(v = 1\text{–}3)$ when $[H_2] < 20\%$. So, the main production mechanism of H^- at atmospheric pressure is found to be neither of these mechanisms. Instead, dissociative attachment of ground state H_2 ((R50): e+$H_2 \rightarrow H^-$+H) results in a generation rate of H^- that is ~1 order of magnitude larger than the rest. This is a consequence of the larger collisionality of the discharge that leads to (1) lower electron mean energy than in low-pressure plasmas and therefore lower generation rates of energetic species such as vibrationally excited $H_2(v'')$ and Rydberg states $H_2(R)$; and (2) collisional relaxation of energetic excited states. As a result, the density ratios of $[H_2(v'')]$ and $[H_2(R)]$ to $[H_2]$ are much lower in atmospheric-pressure plasmas than in their low-pressure counterparts, and hence (R50), instead of (R51)–(R54) and/or (R55), dominates H^- production. Regarding the loss mechanisms for H^- (figure 4(*b*)), collisional detachment by $H_2(v)$ ((R75)–(R77)) dominates at low H_2 concentrations ($[H_2] < 100$ ppm) and (R73), $H^- + H \rightarrow H_2 + e$, becomes the main process at higher H_2 concentrations.

From an application point of view, it is of interest to unravel the mechanisms involved in the production of atomic hydrogen H. The generation and loss mechanisms as a function of the H_2 concentration are shown in figure 5(*a*) and (*b*), respectively. At low hydrogen concentrations ($[H_2] < 10$ ppm), the ion–neutral reactions (mainly (R94): $H_2^+ + He \rightarrow HeH^+ + H$) dominate the generation processes of H. At these low H_2 concentrations, Penning ionization is very effective, leading to the generation of H_2^+, which rapidly reacts with helium atoms to release H. However, higher H density can be obtained when the H_2 content is larger than 50 ppm (figure 2). Under these conditions, the main generation mechanism of H is electron impact dissociation (R23), which reaches a maximum rate at $[H_2]$ ~2%. The decreasing rate at higher H_2 concentrations is attributed to the decrease in both electron density (see figure 1) and electron temperature as more input power is coupled into vibrational excitation of H_2 (section 3.3). Other generation processes, such as electron–ion recombination, electron impact dissociation of $H_2(v)$ and reactions between neutral species, have negligible contribution. At low H_2 concentrations, Penning ionization (R118) and (R121) leads to the loss of atomic H (figure 5(*b*)) but at higher concentrations three-body recombination reactions (mainly (R128) and (R130)) dominate the loss mechanism.

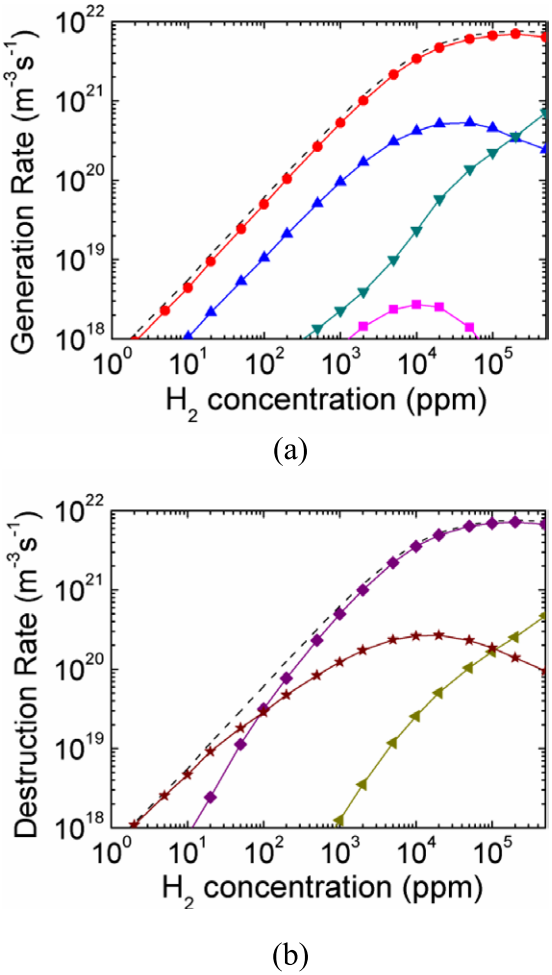

Figure 4. Processes contributing to (*a*) generation and (*b*) loss of H^-; - - - -: total rate; : dissociative attachment of H_2; : dissociative attachment of $H_2(v = 1\text{–}3)$; : dissociative attachment of $H_2(v'')$; : dissociative attachment of $H_2(R)$; : $H^- + H \rightarrow H_2 + e$; : collisional detachment by $H_2(v = 1\text{–}3)$; : recombination.

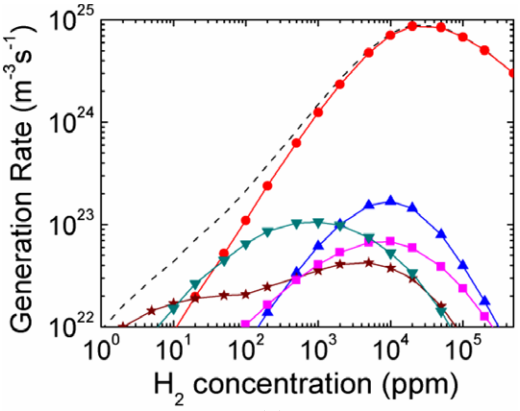

(a)

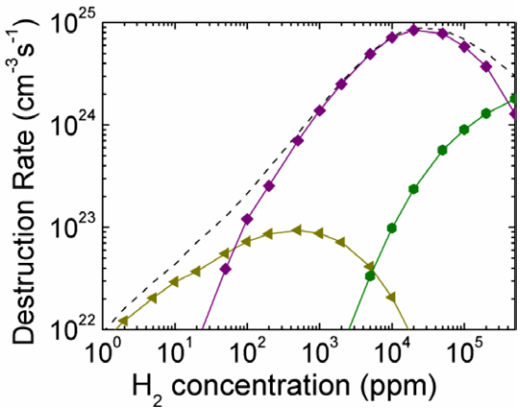

(b)

Figure 5. Processes contributing to (*a*) generation and (*b*) loss of ground state H; - - - -: total rate; : electron impact dissociation of H_2; : electron impact dissociation of $H_2(v)$; : electron–ion recombination; : reactions with neutrals; : ion–neutral reactions; : $2H + He \rightarrow H_2 + He$; : $2H + H_2 \rightarrow 2H_2$; : Penning ionization.

For a H_2 concentration of ∼2% that leads to the maximum H production (figure 1), the production of H is dominated by electron impact dissociation (R23):e+H_2 → 2H+e and balanced by the loss via (R128):2H+He → H_2+He. Therefore, an increase in electron and gas temperature (rate coefficient of (R128) is inversely proportional to the gas temperature) would improve H production efficiency.

3.3. Power dissipation

Figure 6 shows the main power dissipation channels in He+H_2 plasmas as a function of the H_2 concentration. For H_2 concentrations below 2%, most of the power delivered to the plasma is dissipated via elastic (momentum transfer) collisions. This is due to the large collisionality encountered in atmospheric-pressure plasmas and the relative efficient energy transfer due to the low atomic weight of helium. Similar trends have been reported in He+O_2 [14] and He+H_2O [15] plasmas.

At high H_2 concentrations ($[H_2] > 2\%$), however, the main power dissipation channel switches to inelastic processes, in particular to vibrational excitation of H_2. It is noted that

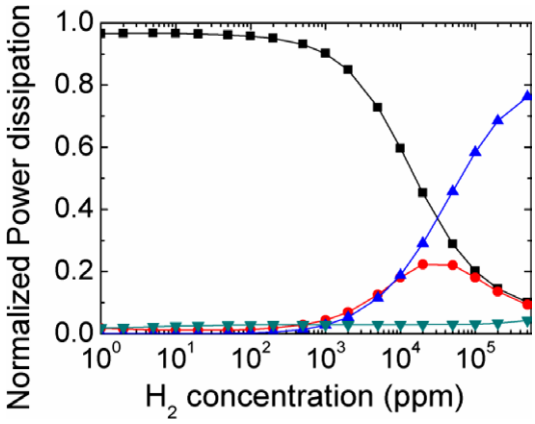

Figure 6. Power dissipation as a function of H_2 concentration; : elastic collisions; : vibrational excitation of H_2; : ion Joule heating; : other inelastic collisions.

vibrational excitation in He+H_2 plasmas is much more efficient than in admixtures of other molecular gases (e.g. He+O_2 [15]) due to the large cross-sections for vibrational excitation of H_2 and the low energy of these states (0.516–1.46 eV for $H_2(v = 1–3)$ [38]). As a result, vibrational excitation becomes the main power dissipation mechanism when $[H_2] > 2\%$ and therefore although vibrational excitation to $H_2(v = 1–3)$ has been neglected in some studies of low-pressure plasmas [7, 39], this should be taken into account in atmospheric-pressure discharges. In fact, the rapid drop in electron density observed in figure 1 is a consequence of the increase in energy lost into vibrational excitation and neglecting vibrational excitation would result in a different electron density trend.

Power coupling into other inelastic collision processes required to maintain the discharge, such as electronic excitation, ionization and dissociation, is most efficient for hydrogen concentrations around ∼2% (figure 6), when ∼24% of the input power is coupled into them.

In addition to the power coupled into the electrons and dissipated via elastic and inelastic collisions (figure 6), 3–4% of the input power is directly coupled to the ions (see the discussion accompanying equations (2) and (3)).

3.4. Main species and chemical reactions

The model used in this study incorporates a fairly large number of species and reactions. While these can be easily handled by a global model, it is of interest to identify a subset of reactions that can capture the main physicochemical processes but with reduced numerical demands. Such a reduced model could then be used in computationally expensive models, such as multi-dimensional fluid models and particle-in-cell simulations.

The criteria used to identify the main species and reactions are the ones detailed in [15]. In brief, once the simulation has reached a steady state, species with density larger than 5% of the total positive ion density are deemed to be important, and reactions with a contribution to particle balance of one key species above 5% are deemed to be key chemical pathways. In addition, some intermediate species that do not reach the threshold density but contribute significantly to the particle

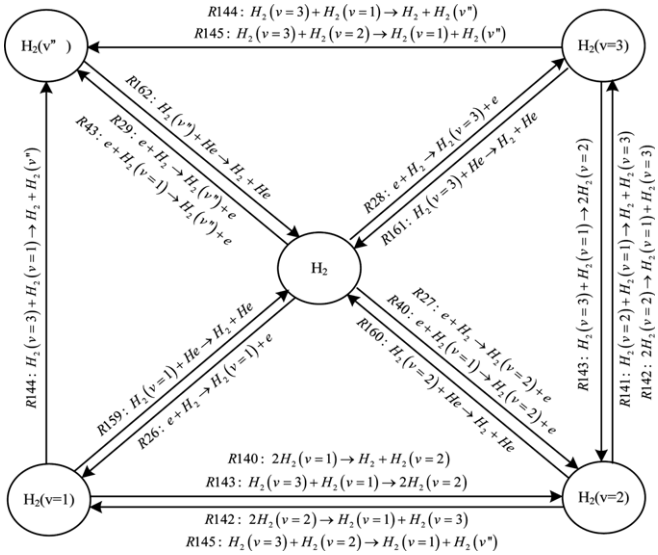

Figure 7. Main reactions for the generation/loss of $H_2(v)$.

balance of a more abundant species are also considered. For example, H_2^+ has a very low density but it is an important precursor of H_3^+ and therefore it is also included.

Applying the above criteria, two chemical sets are proposed. One for He+H_2 plasmas with a low H_2 concentration (RG1) and another one for plasmas with a high H_2 concentration (RG2):

- Regime 1 (RG1): discharges containing 1–5000 ppm of hydrogen. In this regime, plasma species originated from helium are abundant and electron (ion) production is mainly ascribed to Penning processes. The density of hydrogen anions is very low in this regime and the plasma is clearly electropositive. The input power is mainly consumed by momentum transfer collisions between electrons and background helium.
- Regime 2 (RG2): discharges containing 0.5–50% of hydrogen. In this regime, the density of helium-containing ions is negligible. Dissociative attachment and collisional detachment processes are important and vibrational excitation of H_2 molecules absorbs most of the input power.

In total, 15 main species and 41 key reactions are identified for regime RG1, whereas 14 main species and 29 key reactions are proposed for regime RG2. These species and reactions are identified in tables 1, and A1. It is noted that a further reduction can be accomplished if different vibrational states can be combined into an 'effective' vibrational state. This is possible because, as indicated in figure 7, the population of vibrational states does not interact significantly with the rest of the discharge chemistry and electron impact excitation and collisional quenching primarily control their balance.

4. Effect of power modulation on plasma-induced species

The results discussed in previous sections assume that the instantaneous input voltage ($P(t)$) varies according to

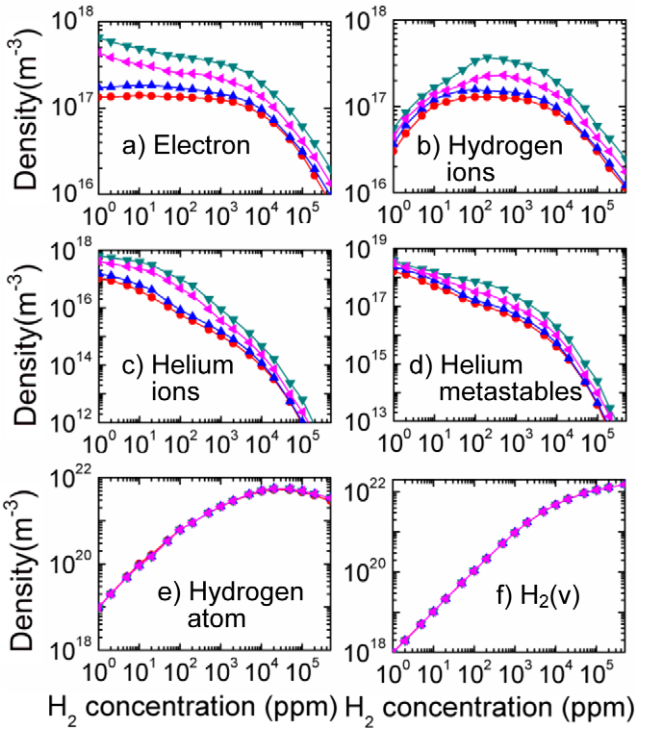

Figure 8. Densities of plasma species for different input power waveforms (40 W cm^{-3}); : constant; : absolute sinusoidal; : pulsed (duty cycle= 50%); : pulsed (duty cycle= 25%).

$P(t) = \frac{\pi}{2} P_{\text{ave}} |\sin(\omega t)|$. This is an approximation of the actual time evolution of the instantaneous power delivered to the discharge and therefore it is important to assess the dependence of the results on this approximation. To this end, four different input power waveforms with the same average input power (40 W cm^{-3}) have been simulated: constant power, absolute value of a sinusoidal waveform, square pulse with a 50% duty cycle and square pulse with a 25% duty cycle. Figure 8 compares the phase-averaged density of various plasma species. For the sake of clarity, the main plasma-induced species (table 1) are grouped into six categories: electrons, helium-containing ions (e.g. He^+, He_2^+ and HeH^+), hydrogen ions (e.g. H^+, H_2^+, H_3^+ and H^-), helium metastables (He^* and He_2^*), atomic hydrogen (H) and vibrational excited hydrogen ($H_2(v)$).

As shown in figure 8, the densities of atomic H and $H_2(v)$ are quite insensitive to the actual evolution of the input power and this is true for species requiring low electron energies for their formation. Differences, however, are found in the average density of excited and charged species. The evolution of the electron temperature during one cycle is shown in figure 9 for each of the four input power waveforms. It can be seen that the maximum electron temperature increases from $T_e \sim 2.5$ eV for the constant input power up to 3.25 eV for the square pulse with 25% duty cycle. Due to the non-linear dependence of excitation/ionization rate on the electron temperature, the pulsed power with 25% duty cycle is the most efficient in generating species that require impact with high-energy electrons, such as helium metastables ($\varepsilon_{\text{th}} = 19.8$ eV), hydrogen ions ($\varepsilon_{\text{th}} = 15.4$ eV) and helium

ions (ε_{th} = 24.6 eV). This also results in an enhancement of electron generation via Penning processes (relaxation of helium metastables) and electron impact ionization of He and H_2. No significant difference is observed in the density of species that require a lower energy.

5. Conclusion

Low-temperature atmospheric-pressure He+H_2 plasmas have been numerically studied by means of a global model over a wide range of H_2 concentrations (1 ppm to 50%). The model incorporates a large set of species and reactions (20 species and 168 chemical reactions), which were identified after an extensive literature review. Two reduced sets of reactions (one for plasmas with a H_2 concentration below 0.5% and one for plasmas with H_2 concentrations above 0.5%) are proposed to minimize the computational demands of the chemistry model while still capturing the main physicochemical processes.

It is found that the plasma density decreases rapidly at higher hydrogen concentrations of $[H_2] > 0.2\%$ due to the increasing energy invested in vibrational excitation of H_2 molecules. H^- is identified as the main anion and its production mechanism differs from that in low-pressure discharges. At atmospheric pressure, and due to the large collisional relaxation of vibrationally excited molecules and Rydberg states, dissociative attachment of ground state hydrogen is found to be the main H^- production mechanism. The density of H^- increases monotonically with H_2 concentration although it remains smaller than the electron density for the conditions studied here.

From an application point of view, it is of interest to identify the conditions that lead to the largest production of atomic H. It is found that this occurs when the hydrogen density is ~2%. At lower H_2 concentrations there is less hydrogen available in the gas whereas at higher concentrations the increasing energy lost in vibrational excitation and the increase in three-body recombination involving H_2 result in a less efficient H production.

Due to the large collisionality of atmospheric-pressure plasmas, the electron temperature is expected to be markedly time-modulated. It is found that although the input power waveform has a significant impact on the density of excited and ionic species, species with low energy threshold for formation such as hydrogen atoms and vibrational excited states of H_2 are fairly insensitive to the actual waveform of the input power.

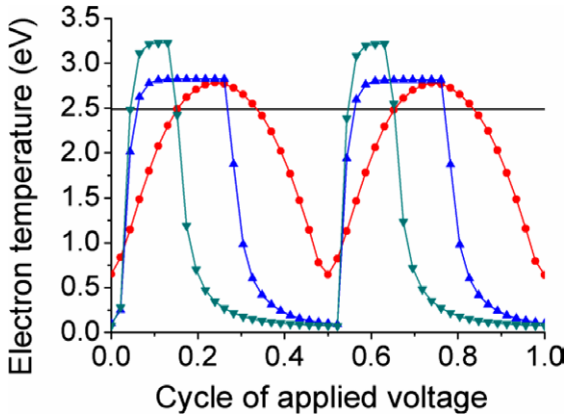

Figure 9. Evolution of electron temperature in an applied voltage cycle; ——: constant; —●—: sinusoidal; —▲—: pulsed (duty cycle= 50%); —▼—: pulsed (duty cycle= 25%).

Acknowledgments

The authors would like to thank Dr Peter Bruggeman (Eindhoven University, The Netherlands) for fruitful discussions related to this work. This work was supported by the Fundamental Research Funds for the Central Universities of China, the State Key Laboratory of Electrical Insulation and Power Equipment (No EIPE11108 and EIPE12301) and the Engineering Physical Science Research Council (UK).

Appendix

Chemical reactions included in the models are listed in table A1.

Table A1. Chemical reactions included in the models.

No	Reaction[a]	Rate coefficient[b]	Note[c]	Ref
(1)	$e + He \rightarrow He + e$	$f(T_e)$	S	[40]
(2)	$e + H_2 \rightarrow H_2 + e$	$f(T_e)$	S2	[38]
(3)	$e + He \rightarrow He^+ + 2e$	$f(T_e)$	S1	[40]
(4)	$e + He^* \rightarrow He^+ + 2e$	$f(T_e)$	S1	[40]
(5)	$e + He_2^* \rightarrow He_2^+ + 2e$	$9.75 \times 10^{-10} T_e^{0.71} \exp\left(-\frac{3.4}{T_e}\right)$	S1	[23]
(6)	$e + H \rightarrow H^+ + 2e$	$f(T_e)$	S	[41]
(7)	$e + H(n = 2) \rightarrow H^+ + 2e$	$f(T_e)$		[41]
(8)	$e + H(n = 3) \rightarrow H^+ + 2e$	$f(T_e)$		[41]
(9)	$e + H_2 \rightarrow H_2^+ + 2e$	$f(T_e)$	S	[41]
(10)	$e + H_2 \rightarrow H^+ + H + 2e$	$f(T_e)$	S2	[41]
(11)	$e + H^- \rightarrow H + 2e$	$f(T_e)$		[41]
(12)	$e + H_2(v = 1) \rightarrow H_2^+ + 2e$	$f(T_e)$		[45]
(13)	$e + H_2(v = 1) \rightarrow H^+ + H + 2e$	$f(T_e)$		[45]
(14)	$e + H_2(v = 2) \rightarrow H_2^+ + 2e$	$f(T_e)$		[45]
(15)	$e + H_2(v = 2) \rightarrow H^+ + H + 2e$	$f(T_e)$		[45]
(16)	$e + H_2(v = 3) \rightarrow H_2^+ + 2e$	$f(T_e)$		[45]

Table A1. Continued.

No	Reaction[a]	Rate coefficient[b]	Note[c]	Ref
(17)	$e + H_2(v = 3) \rightarrow H^+ + H + 2e$	$f(T_e)$		[45]
(18)	$e + He \rightarrow He^* + e$	$f(T_e)$	S1	[40]
(19)	$e + He^* \rightarrow He + e$	$f(T_e)$		[40][e]
(20)	$e + He_2^* \rightarrow 2He + e$	3.8×10^{-9}		[42]
(21)	$e + H \rightarrow H(n = 2) + e$	$f(T_e)$		[41]
(22)	$e + H \rightarrow H(n = 3) + e$	$f(T_e)$		[41]
(23)	$e + H_2 \rightarrow 2H + e$	$f(T_e)$	S	[41]
(24)	$e + H_2 \rightarrow H + H(n = 2) + e$	$f(T_e)$		[43]
(25)	$e + H_2 \rightarrow H + H(n = 3) + e$	$f(T_e)$		[43]
(26)	$e + H_2 \rightarrow H_2(v = 1) + e$	$f(T_e)$	S	[38]
(27)	$e + H_2 \rightarrow H_2(v = 2) + e$	$f(T_e)$	S	[38]
(28)	$e + H_2 \rightarrow H_2(v = 3) + e$	$f(T_e)$	S	[38]
(29)	$e + H_2 \rightarrow H_2(v'') + e$	$f(T_e)$	S2	[41, 44]
(30)	$e + H_2 \rightarrow H_2(R) + e$	$f(T_e)$		[38]
(31)	$e + H_2(v = 1) \rightarrow 2H + e$	$f(T_e)$		[45]
(32)	$e + H_2(v = 1) \rightarrow H + H(n = 2) + e$	$f(T_e)$		[45]
(33)	$e + H_2(v = 1) \rightarrow H + H(n = 3) + e$	$f(T_e)$		[45]
(34)	$e + H_2(v = 2) \rightarrow 2H + e$	$f(T_e)$		[45]
(35)	$e + H_2(v = 2) \rightarrow H + H(n = 2) + e$	$f(T_e)$		[45]
(36)	$e + H_2(v = 2) \rightarrow H + H(n = 3) + e$	$f(T_e)$		[45]
(37)	$e + H_2(v = 3) \rightarrow 2H + e$	$f(T_e)$		[45]
(38)	$e + H_2(v = 3) \rightarrow H + H(n = 2) + e$	$f(T_e)$		[45]
(39)	$e + H_2(v = 3) \rightarrow H + H(n = 3) + e$	$f(T_e)$		[45]
(40)	$e + H_2(v = 1) \rightarrow H_2(v = 2) + e$	$f(T_e)$	S1	[45]
(41)	$e + H_2(v = 1) \rightarrow H_2(v = 3) + e$	$f(T_e)$		[45]
(42)	$e + H_2(v = 2) \rightarrow H_2(v = 3) + e$	$f(T_e)$		[45]
(43)	$e + H_2(v = 1) \rightarrow H_2(v'') + e$	$f(T_e)$	S2	[45]
(44)	$e + H_2(v = 2) \rightarrow H_2(v'') + e$	$f(T_e)$		[45]
(45)	$e + H_2(v = 3) \rightarrow H_2(v'') + e$	$f(T_e)$		[45]
(46)	$e + H_2(v = 1) \rightarrow H_2(R) + e$	$f(T_e)$		[d]
(47)	$e + H_2(v = 2) \rightarrow H_2(R) + e$	$f(T_e)$		[d]
(48)	$e + H_2(v = 3) \rightarrow H_2(R) + e$	$f(T_e)$		[d]
(49)	$e + H \rightarrow H^-$	$3.46 \times 10^{-16} T_e^{0.5}$		
(50)	$e + H_2 \rightarrow H^- + H$	$f(T_e)$	S2	[43]
(51)	$e + H_2(v = 1) \rightarrow H + H^-$	$f(T_e)$		[47]
(52)	$e + H_2(v = 2) \rightarrow H + H^-$	$f(T_e)$		[47]
(53)	$e + H_2(v = 3) \rightarrow H + H^-$	$f(T_e)$		[47]
(54)	$e + H_2(v'') \rightarrow H^- + H$	$f(T_e)$		[41]
(55)	$e + H_2(R) \rightarrow H + H^-$	6×10^{-5}		[48]
(56)	$e + He^+ \rightarrow He^*$	$6.76 \times 10^{-13} T_e^{-0.5}$		[12]
(57)	$2e + He^+ \rightarrow He^* + e$	$7.8 \times 10^{-38} (T_e/T_g)^{-4.4}$		[23]
(58)	$e + He^+ + M \rightarrow He^* + M$	$7.4 \times 10^{-35} (T_e/T_g)^{-2}$		[49]
(59)	$e + He_2^+ \rightarrow He^* + He$	$7.12 \times 10^{-15} (T_e/T_g)^{-1.5}$		[50]
(60)	$2e + He_2^+ \rightarrow He^* + He + e$	2.8×10^{-20}		[42]
(61)	$2e + He_2^+ \rightarrow He_2^* + e$	1.2×10^{-21}		[42]
(62)	$e + He_2^+ + M \rightarrow He^* + He + M$	3.5×10^{-27}		[42]
(63)	$e + He_2^+ + M \rightarrow He_2^* + M$	1.5×10^{-27}		[42]
(64)	$e + HeH^+ \rightarrow H + He$	$1.1 \times 10^{-9} T_e^{-0.6}$		[46]
(65)	$e + H^+ \rightarrow H$	$2.62 \times 10^{-13} T_e^{-0.5}$		[51]
(66)	$2e + H^+ \rightarrow e + H$	$8.8 \times 10^{-27} T_e^{-4.5}$		[52]
(67)	$e + H_2^+ \rightarrow H + H^+ + e$	$1.89 \times 10^{-7} T_e^{-0.13} \exp\left(-\frac{2.3}{T_e}\right)$		[43]
(68)	$e + H_2^+ \rightarrow H + H(n = 3)$	$5.66 \times 10^{-8} T_e^{-0.6}$		[43]
(69)	$e + H_3^+ \rightarrow 3H$	$4.15 \times 10^{-8} T_e^{-0.4}$		[41]
(70)	$e + H_3^+ \rightarrow H(n = 2) + H_2(v'')$	$4.15 \times 10^{-8} T_e^{-0.4}$		[41]
(71)	$e + H_3^+ + M \rightarrow H_2 + H + M$	2.8×10^{-25}	S	[53]
(72)	$e + H_3^+ \rightarrow H^+ + 2H + e$	$1.75 \times 10^{-8} T_e^{0.95} \exp\left(-\frac{10.5}{T_e}\right)$		[41]
(73)	$H^- + H \rightarrow H_2 + e$	1.3×10^{-9}	S2	[46]
(74)	$H^- + H \rightarrow 2H + e$	$6 \times 10^{-15} (T_g/300)^{3.5}$		[54]
(75)	$H^- + H_2(v = 1) \rightarrow H_2 + H + e$	5.7×10^{-12}		[55, 56]
(76)	$H^- + H_2(v = 2) \rightarrow H_2 + H + e$	6×10^{-11}		[55, 56]

Table A1. Continued.

No	Reaction[a]	Rate coefficient[b]	Note[c]	Ref
(77)	$H^- + H_2(v = 3) \rightarrow H_2 + H + e$	1.6×10^{-10}		[55, 56]
(78)	$H^- + He^* \rightarrow H + He + e$	2×10^{-10}		[57]
(79)	$H^- + He_2^* \rightarrow H + 2He + e$	2×10^{-10}		[57]
(80)	$He^+ + 2He \rightarrow He_2^+ + He$	$1.4 \times 10^{-31}(T_g/300)^{-0.6}$	S1	[23]
(81)	$He^+ + H \rightarrow H^+ + He$	1.9×10^{-15}		[46]
(82)	$He^+ + H \rightarrow HeH^+$	$1.58 \times 10^{-15}(T_g/300)^{-0.3}$		[58]
(83)	$He^+ + H_2 \rightarrow H^+ + H + He$	$3.7 \times 10^{-14}\exp(-35/T_g)$		[46]
(84)	$He^+ + H_2 \rightarrow H_2^+ + He$	7.2×10^{-15}		[46]
(85)	$He_2^+ + H \rightarrow H^+ + 2He$	3.5×10^{-10}	S1	f
(86)	$He_2^+ + H_2 \rightarrow H_2^+ + 2He$	3.5×10^{-10}	S1	[54]
(87)	$He_2^+ + H_2 \rightarrow HeH^+ + H + He$	1.76×10^{-10}	S1	[54]
(88)	$HeH^+ + H \rightarrow H_2^+ + He$	9.1×10^{-10}	S1	[46]
(89)	$HeH^+ + H_2 \rightarrow H_3^+ + He$	1.5×10^{-9}	S1	[46]
(90)	$H^+ + He \rightarrow HeH^+$	$8.4 \times 10^{-19}(T_g/300)^{-4.5}$		[59]
(91)	$H^+ + 2H_2 \rightarrow H_3^+ + H_2$	$3.1 \times 10^{-29}(T_g/300)^{-0.5}$	S2	[54]
(92)	$H^+ + H_2 + He \rightarrow H_3^+ + He$	1.5×10^{-29}	S	[60]
(93)	$H^+ + H + M \rightarrow H_2^+ + M$	1×10^{-34}		[61]
(94)	$H_2^+ + He \rightarrow HeH^+ + H$	1.3×10^{-10}	S1	[46]
(95)	$H_2^+ + H \rightarrow H^+ + H_2$	6.39×10^{-10}		[52]
(96)	$H_2^+ + H_2 \rightarrow H_3^+ + H$	2.1×10^{-9}	S2	[54]
(97)	$H_3^+ + He^* \rightarrow H_2 + H^+ + He$	1×10^{-10}		[57]
(98)	$H_3^+ + He_2^* \rightarrow H_2 + H^+ + 2He$	1×10^{-10}		[57]
(99)	$H^- + He^+ \rightarrow H + He$	$2.3 \times 10^{-7}(T_g/300)^{-0.5}$		[46]
(100)	$H^- + He_2^+ \rightarrow H + 2He$	$2 \times 10^{-7}(T_g/300)^{-0.5}$		[28]
(101)	$H^- + HeH^+ \rightarrow H_2 + He$	1×10^{-7}		[28]
(102)	$H^- + H^+ \rightarrow H(n = 2) + H$	$9 \times 10^{-11}(T_g/300)^{0.83}$		[49]
(103)	$H^- + H^+ \rightarrow H(n = 3) + H$	$1.8 \times 10^{-7}(T_g/300)^{-0.5}$		[49]
(104)	$H^- + H_2^+ \rightarrow H + H_2$	$2 \times 10^{-7}(T_g/300)^{-0.5}$		[54]
(105)	$H^- + H_3^+ \rightarrow 2H_2$	$2 \times 10^{-7}(T_g/300)^{-0.5}$		[54]
(106)	$H^- + He^+ + M \rightarrow H + He + M$	$2 \times 10^{-25}(T_g/300)^{-2.5}$		[28]
(107)	$H^- + He_2^+ + M \rightarrow H + 2He + M$	$2 \times 10^{-25}(T_g/300)^{-2.5}$		[28]
(108)	$H^- + H^+ + M \rightarrow 2H + M$	$2 \times 10^{-25}(T_g/300)^{-2.5}$		[28]
(109)	$H^- + H_2^+ + M \rightarrow H + H_2 + M$	$2 \times 10^{-25}(T_g/300)^{-2.5}$		[28]
(110)	$H^- + H_3^+ + M \rightarrow 2H + H_2 + M$	$2 \times 10^{-25}(T_g/300)^{-2.5}$	S2	[28]
(111)	$H^- + HeH^+ + M \rightarrow 2H + He + M$	$2 \times 10^{-25}(T_g/300)^{-2.5}$		[28]
(112)	$2He^* \rightarrow He_2^+ + e$	$2.03 \times 10^{-9}(T_g/300)^{0.5}$	S1	[23]
(113)	$2He^* \rightarrow He^+ + He + e$	$8.7 \times 10^{-10}(T_g/300)^{0.5}$	S1	[23]
(114)	$He^* + He_2^* \rightarrow He^+ + 2He + e$	5×10^{-10}	S1	[42]
(115)	$He^* + He_2^* \rightarrow He_2^+ + He + e$	2×10^{-9}	S1	[42]
(116)	$2He_2^* \rightarrow He^+ + 3He + e$	3×10^{-10}	S1	[42]
(117)	$2He_2^* \rightarrow He_2^+ + 2He + e$	1.2×10^{-9}	S1	[42]
(118)	$He^* + H \rightarrow H^+ + He + e$	1.1×10^{-9}	S1	[44]
(119)	$He^* + H_2 \rightarrow H_2^+ + He + e$	2.9×10^{-11}	S1	[62, 63]
(120)	$He^* + H_2 \rightarrow H + HeH^+ + e$	3×10^{-12}	S1	[62, 63]
(121)	$He_2^* + H \rightarrow 2He + H^+ + e$	2.2×10^{-10}	S1	f
(122)	$He_2^* + H_2 \rightarrow H_2^+ + 2He + e$	2.2×10^{-10}	S1	[64]
(123)	$H(n = 2) + H_2 \rightarrow H_3^+ + e$	$1.4 \times 10^{-11}(T_g/300)^{0.5}$		[65]
(124)	$H(n = 3) + H_2 \rightarrow H_3^+ + e$	$4.83 \times 10^{-10}(T_g/300)^{0.5}$		[54]
(125)	$He^* + He \rightarrow 2He$	5.8×10^{-15}	S1	[66]
(126)	$He^* + 2He \rightarrow He_2^* + He$	2×10^{-34}	S1	[50]
(127)	$2H \rightarrow H_2$	$6.04 \times 10^{-33}(T_g/298)^{-1}$		[67]
(128)	$2H + He \rightarrow He + H_2$	$5.8 \times 10^{-33}(T_g/300)^{-1}$	S	[68]
(129)	$3H \rightarrow H + H_2$	$6 \times 10^{-31}(T_g/300)^{-1}$		[52]
(130)	$2H + H_2 \rightarrow 2H_2$	$8.1 \times 10^{-33}(T_g/300)^{-0.6}$	S2	[68]
(131)	$He_2^* + M \rightarrow 2He + M$	1.5×10^{-15}	S1	[50]
(132)	$H(n = 2) + He \rightarrow H + He$	2.7×10^{-13}		[69]
(133)	$H(n = 2) + H_2 \rightarrow H + H_2$	2.1×10^{-11}		[52]
(134)	$H(n = 3) + He \rightarrow H + He$	1×10^{-11}		[70]
(135)	$H(n = 3) + H_2 \rightarrow H + H_2$	2×10^{-9}		[70]
(136)	$H_2(v = 1) + H_2 \rightarrow 2H_2$	$1 \times 10^{-16}(T_g/300)^{4.5}$		[71]
(137)	$H_2(v = 2) + H_2 \rightarrow H_2 + H_2(v = 1)$	2.2×10^{-16}		[72]

Table A1. Continued.

No	Reaction[a]	Rate coefficient[b]	Note[c]	Ref
(138)	$H_2(v=3)+H_2 \rightarrow H_2+H_2(v=2)$	4.9×10^{-16}		[72]
(139)	$H_2(v'')+H_2 \rightarrow H_2+H_2(v=3)$	1.07×10^{-15}		[72][g]
(140)	$H_2(v=1)+H_2(v=1) \rightarrow H_2+H_2(v=2)$	7.6×10^{-13}	S	[73]
(141)	$H_2(v=2)+H_2(v=1)$ $H_2+H_2(v=3)$	1.1×10^{-12}	S	[73]
(142)	$H_2(v=2)+H_2(v=2) \rightarrow H_2(v=1)+H_2(v=3)$	2.28×10^{-12}	S2	[72]
(143)	$H_2(v=3)+H_2(v=1) \rightarrow H_2(v=2)+H_2(v=2)$	8.1×10^{-13}	S2	[73]
(144)	$H_2(v=3)+H_2(v=1) \rightarrow H_2+H_2(v'')$	8.4×10^{-13}	S2	[72]
(145)	$H_2(v=3)+H_2(v=2) \rightarrow H_2(v=1)+H_2(v'')$	2.9×10^{-12}	S2	[72]
(146)	$H_2(v=3)+H_2(v=3) \rightarrow H_2(v=2)+H_2(v'')$	4.56×10^{-12}		[72]
(147)	$H_2(v=1)+H_2(v'') \rightarrow H_2(v=2)+H_2(v=3)$	4.7×10^{-13}		[72][g]
(148)	$H_2(v=2)+H_2(v'') \rightarrow H_2(v=3)+H_2(v=3)$	1.6×10^{-12}		[72][g]
(149)	$H_2(v=1)+H \rightarrow H+H_2$	4.2×10^{-14}		[74]
(150)	$H_2(v=2)+H \rightarrow H+H_2$	5.9×10^{-13}		[74]
(151)	$H_2(v=2)+H \rightarrow H+H_2(v=1)$	3×10^{-13}		[74]
(152)	$H_2(v=3)+H \rightarrow H+H_2$	1.5×10^{-12}		[74]
(153)	$H_2(v=3)+H \rightarrow H+H_2(v=1)$	1.6×10^{-12}		[74]
(154)	$H_2(v=3)+H \rightarrow H+H_2(v=2)$	2×10^{-12}		[74]
(155)	$H_2(v'')+H \rightarrow H+H_2$	4.3×10^{-12}		[74][g]
(156	$H_2(v'')+H \rightarrow H+H_2(v=1)$	4.2×10^{-12}		[74][g]
(157)	$H_2(v'')+H \rightarrow H+H_2(v=2)$	4.9×10^{-12}		[74][g]
(158)	$H_2(v'')+H \rightarrow H+H_2(v=3)$	5.5×10^{-12}		[74][g]
(159)	$H_2(v=1)+He \rightarrow H_2+He$	$2\times10^{-17}(T_g/300)^{2.9}$	S	[75]
(160)	$H_2(v=2)+He \rightarrow H_2+He$	$1.05\times10^{-16}(T_g/300)^{3}$	S	[75]
(161)	$H_2(v=3)+He \rightarrow H_2+He$	$3.9\times10^{-16}(T_g/300)^{3.3}$	S	[75]
(162)	$H_2(v'')+He \rightarrow H_2+He$	$1.1\times10^{-15}(T_g/300)^{3.7}$	S2	[75]
(163)	$H_2(R)+H_2 \rightarrow H_2+2H$	1.88×10^{-9}		[36, 76]
(164)	$H_2(R)+He \rightarrow 2H+He$	8×10^{-10}		[77]
(165)	$H(n=2) \rightarrow H+h\upsilon$	$4.7\times10^{8}\ s^{-1}$		[63]
(166)	$H(n=3) \rightarrow H+h\upsilon$	$5.57\times10^{7}\ s^{-1}$		[63]
(167)	$H(n=3) \rightarrow H(n=2)+h\upsilon$	$4.41\times10^{7}\ s^{-1}$		[63]
(168)	$H_2(R) \rightarrow H_2+h\upsilon$	$1\times10^{6}\ s^{-1}$		[37]

[a] He^* represents $He(2^3S)$ and $He(2^1S)$; He_2^* represents $He_2(a\,^3\Sigma_u^+)$; $H_2(v'')$ represents $H_2(v\geqslant 4)$; $H_2(R)$ represents Rydberg states of H_2; *M* represents the background gases helium and hydrogen.
[b] Rate coefficients have units of $cm^3\ s^{-1}$ for two-body reactions and $cm^6\ s^{-1}$ for three-body reactions; T_e has units eV; T_g has units K. $f(T_e)$ indicates that the rate coefficient is obtained using the cross-section from the indicated reference.
[c] S represents the main reaction in the whole range of hydrogen concentrations. S1: main reactions in RG1; S2: main reactions in RG2; S3: main reactions in RG3.
[d] Cross-section estimated by shifting the ground state cross-section of H_2 by the excitation threshold.
[e] Superelastic cross-section calculated using detailed balance.
[f] Estimated same as H_2.
[g] Using the rate coefficient of $H_2(v=4)$ for $H_2(v'')$.

References

[1] Goossens O, Dekempeneer E, Vangeneugden D, Leest de R V and Leys C 2001 *Surf. Coat. Technol.* **142–144** 474
[2] Hsieh J H and Li C 2006 *Thin Solid Films* **504** 101
[3] Ohmi H, Kakiuchi H, Nishijima K, Watanabe H and Yasutake K 2006 *Japan. J. Appl. Phys.* **45** 8488
[4] Koo I G, Lee M S and Lee W M 2006 *Thin Solid Films* **506–507** 350
[5] Nagai M, Hori M and Goto T 2005 *J. Appl. Phys.* **97** 123304
[6] Chaudhary K, Inomata K, Yoshimoto M and Koinuma H 2003 *Mater. Lett.* **57** 3406
[7] Hagelaar G J M and Kroesen G M W 2000 *J. Appl. Phys.* **88** 2252
[8] Harutyunyan A R, Chen G, Paronyan T M, Pigos E M, Kuznetsov O A, Hewaparakrama K, Kim S M, Zakharov D, Stach E A and Sumanasekera G U 2009 *Science* **326** 116
[9] Matsushita A, Nagai M, Yamakawa K, Hiramatsu M, Sakai A, Hori M, Goto T and Zaima S 2004 *Japan. J. Appl. Phys.* **43** 424

[10] Kim S J, Lieberman M A, Lichtenberg A J and Gumundsson J T 2006 *J. Vac. Sci. Technol.* A **24** 2025
[11] Lieberman M A and Lichtenberg A J 2005 *Principles of Plasma Discharges and Materials Processing* 2nd edn (New York: Wiley)
[12] Stafford D S and Kushner M J 2004 *J. Appl. Phys.* **96** 2451
[13] Park G, Lee H, Kim G and Lee J K 2008 *Plasma Process. Polym.* **5** 569
[14] Liu D X, Rong M G, Wang X H, Iza F, Kong M G and Bruggeman P 2010 *Plasma Process. Polym.* **7** 846
[15] Liu D X, Bruggeman P, Iza F, Rong M Z and Kong M G 2010 *Plasma Sources Sci. Technol.* **19** 025018
[16] Liu D X, Iza F, Wang X H, Kong M G and Rong M Z 2011 *Appl. Phys. Lett.* **98** 221501
[17] Walsh J L, Liu D X, Iza F, Rong M Z and Kong M G 2010 *J. Phys. D: Appl. Phys.* **43** 032001
[18] Gudmundsson J T and Thorsteinsson E G 2007 *Plasma Sources Sci. Technol.* **16** 399
[19] Iza F, Lee J K and Kong M G 2007 *Phys. Rev. Lett.* **99** 075004
[20] Liu D W, Iza F and Kong M G 2009 *Appl. Phys. Lett.* **95** 031501
[21] Yang A J, Wang X H, Rong M Z, Liu D X, Iza F and Kong M G 2011 *Phys. Plasmas* **18** 113503
[22] Veatch G E and Oskam H J 1973 *Phys. Rev.* A **8** 389
[23] Wang Q, Economou D J and Donnelly V M 2006 *J. Appl. Phys.* **100** 023301
[24] Lazzaroni C, Chabert P, Lieberman M A, Lichtenberg A J and Leblanc A 2012 *Plasma Sources Sci. Technol.* **21** 035013
[25] 2013 *MATLAB* version 8.1.0.604 The MathWorks Inc., Natick, MA
[26] Hagelaar G J M and Pitchford L C 2005 *Plasma Sources Sci. Technol.* **14** 722
[27] Kushner M J 1999 *Bull. Am. Phys. Soc.* **44** 63
[28] Kossyi I A, Kostinsky A Y, Matveyev A A and Silakov V P 1992 *Plasma Sources Sci. Technol.* **1** 207
[29] Martens T, Bogaerts A, Brok W J M and Dijk J V 2008 *Appl. Phys. Lett.* **92** 041504
[30] Bruggeman P, Iza F, Lauwers D and Gonzalvo Y A 2010 *J. Phys. D: Appl. Phys.* **43** 012003
[31] Qian M, Ren C, Wang D, Zhang J and Wei G 2010 *J. Appl. Phys.* **107** 063303
[32] Koo G, Cho J H and Lee W M 2008 *Plasma Process. Polym.* **5** 161
[33] Zhou Q, Cheng C and Meng Y 2009 *Plasma Sci. Technol.* **11** 560
[34] Nojima H *et al* 2007 *J. Phys. D: Appl. Phys.* **40** 501
[35] Patnaik P 2007 *A Comprehensive Guide to the Hazardous Properties of Chemical Substances* (Hoboken, NJ: Wiley)
[36] Hassouni K, Gicquel A and Capitelli M 1998 *Chem. Phys. Lett.* **290** 502
[37] Capitelli M and Gorse C 2005 *IEEE Trans. Plasma Sci.* **33** 1832
[38] Phelps A V1985 *JILA Information Center Report* No 28
[39] Mendez I, Grodillo-Vazquez F J, Herrero V J and Tanarro I 2006 *J. Phys. Chem.* A **110** 6060
[40] BOLSIG+ software version 1.1. 2008 www.siglo-kinema.com/technical.htm
[41] Janev R K, Langer W D, Evans J K and Post J D E 1987 *Elementary Processes in Hydrogen–Helium Plasmas: Cross Sections and Reaction Rate Coefficients* (Berlin: Springer)
[42] Deloche R, Monchicourt P, Cheret M and Lambert F 1976 *Phys. Rev.* A **13** 1140
[43] Tawara H, Itikawa Y, Nishimura H and Youshino M 1990 *J. Phys. Chem. Ref. Data* **19** 617
[44] Hagelaar G J M and Kroesen G M W 2000 *J. Appl. Phys.* **88** 2252
[45] Celiberto R, Janev R K, Laricchiuta A, Capitelli M, Wadehra J M and Atems D E 2001 *At. Data Nucl. Data Tables* **77** 161
[46] Millar T J, Farquhar P R A and Willacy K 1997 *Astron. Astrophys. Suppl. Ser.* **121** 139
[47] Gallup G A, Xu Y and Fabrikant I I 1998 *Phys. Rev.* A **57** 2596
[48] Daskos P G, Pinnaduwage L A and Kielkopf J F 1997 *Phys. Rev.* A **55** 4131
[49] Konstantinovskii R S, Shibkov V M and Shibkova L V 2005 *Kinet. Catal.* **46** 775
[50] Golubovskii Y B, Maiorov V A, Behnke J and Behnke J F 2003 *J. Phys. D: Appl. Phys.* **36** 39
[51] Salabas A, Marques L, Jolly J, Gousset G and Alves L L 2004 *J. Appl. Phys.* **95** 4605
[52] Giuliani J L, Shamamian V A, Thomas R E, Apruzese J P, Mulbrandon M, Rudder R A, Hendry R C and Robson A E 1999 *IEEE Trans. Plasma Sci.* **27** 1317
[53] Glosik J J, Korolov I, Plasil R, Novotny O, Kotrik T, Hlavenka P, Varju J, Greene C H, Kokoouline V and Mikhailov I A 2008 *J. Phys. B: At. Mol. Opt. Phys.* **41** 191001
[54] Hassouni K, Grotjohn T A and Gicquel A 1999 *J. Appl. Phys.* **86** 134
[55] Phelps A V 1990 *J. Phys. Chem. Ref. Data* **19** 653
[56] Huq M S, Doverspike L D and Champion R L 1983 *Phys. Rev.* A **27** 2831
[57] Vidmar R J and Stalder K R 2004 *Final Report prepared for Air Force Office of Scientific Research* Report No AFRLSRARRE040123, Contract No F49620-01-1-0414
[58] Kraemer W P, Spirko V and Jurek M 1995 *Chem. Phys. Lett.* **236** 177
[59] Jurek M, Spirko V and Kraemer W P 1995 *Chem. Phys.* **193** 287
[60] McLain J L, Poterya V, Molek C D, Babcock L M and Adams N G 2004 *J. Phys. Chem.* A **108** 6704
[61] Soloshenko I A, Tsiolko V V, Khomich V A, Bazhenov V Y, Ryabtsev A V, Schedrin A I and Mikhno I L 2002 *IEEE Trans. Plasma Sci.* **30** 1440
[62] Adams N G, Bohme D K and Ferguson E E 1970 *J. Chem. Phys.* **52** 5101
[63] Ivanov V A and Skoblo Y E 2005 *Opt. Spectrosc.* **98** 811
[64] Takao S, Kogoma M, Oka T, Imamura M and Arai S 1980 *J. Chem. Phys.* **73** 148
[65] Specht L T, Foster K D and Muschlitz J E E 1975 *J. Chem. Phys.* **63** 1582
[66] Sommerer T J and Kushner M J 1992 *J. Appl. Phys.* **71** 1654
[67] *NIST Chemical Kinetic Database* http://kinetics.nist.gov/kinetics/index.jsp
[68] *GRI-MECH 3 Reaction Rate Database* www.me.berkeley.edu/gri-mech/
[69] Zuev V S, Kanaev A V and Mikheev L D 1984 *Sov. J. Quantum Electron.* **14** 135
[70] Bittner J, Kohse-hoinghaus K, Meier U and Just T 1988 *Chem. Phys. Lett.* **143** 571
[71] Flower D R and Roueff E 1998 *J. Phys. B: At. Mol. Opt. Phys.* **31** 2935
[72] Loureiro J and Ferreira C M 1989 *J. Phys. D: Appl. Phys.* **22** 1680
[73] Billing G D and Fisher E R 1976 *Chem. Phys.* **18** 225
[74] Gorse C, Capitelli M, Bacal M and Bretagne J 1987 *Chem. Phys.* **117** 177
[75] Balakrishnan N, Forrey R C and Dalgarno A 1998 *Phys. Rev. Lett.* **80** 3224
[76] Wedding A B and Phelps A V 1988 *J. Chem. Phys.* **89** 2965
[77] Kligler D J and Rhodes C K 1978 *Phys. Rev. Lett.* **40** 309